# MAGNETIC FIELD COMPUTATIONS OF FRINGE FIELDS BETWEEN A DIPOLE AND A QUADRUPOLE MAGNET

L. Rinolfi, CERN, CH-1211 Geneva 23, Switzerland
K. Preis, K.H. Richter, H. Stögner, IGTE, Austria

The aim of this paper is to present the results, of 3-D calculations, on the interferences between a dipole and a quadrupole magnet in the CERN Antiproton Collector lattice.

## Introduction

The uniformity of field in the ends of the good field region of a dipole is affected by the proximity of other magnets. In the ACOL ring where magnets are short and of large aperture [1], this effect deserves particular attention [2].

With a configuration as shown in Figure 1, it was planned to study:

- the end field of the dipole in the presence of an unexcited quadrupole;
- the end field of the quadrupole in the presence of an unexcited dipole;
- the end fields of the dipole and the quadrupole with both at nominal current.

We describe here the first case where the quadrupole is simulated by a plate with the same permeability $\mu_r$ as the dipole iron. The angle is $7.5^{\circ}$ and the distance between the plate and the centre of the dipole face is 0.495 m (Fig. 2). For comparison, computations were made with a plate parallel to the end face of the dipole [3].

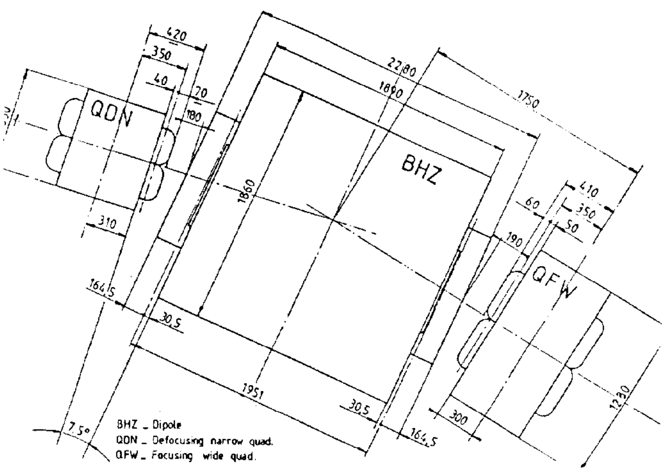


Fig. 1: Dipole quadrupole arrangement in the ACOL lattice

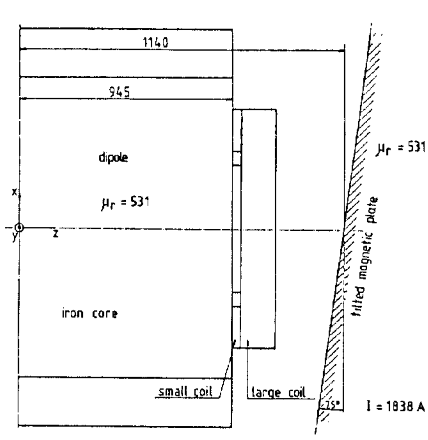


Fig. 2: Top view of dipole and tilted plate

## Finite element software package

To calculate the magnetic field distribution within the dipole, the Finite Element Method (FEM) is used. The three-dimensional (3-D) software package for numerical calculations was developed at IGTE (Institute of foundations and theory of electrical engineering) at the Technical University of Graz, Austria. The software package is based on 20-noded higher order isoparametric finite elements [4].

## Mathematical description

The field problem under consideration can be described by the well-known Maxwell equations:

$$\mathrm{curl}\,\vec{H} = \vec{J}_e \ (1); \mathrm{curl}\,\vec{E} = \vec{0} \ (2); \mathrm{div}\,\vec{B} = 0 \ (3); \vec{B} = \mu\vec{H} \ (4)$$

where $\vec{J}_e$ is the imposed current density, $\vec{E}$ the electric field, $\vec{H}$ and $\vec{B}$ are the magnetic excitation and magnetic flux density, respectively. The magnetic permeability $\mu_r$ is assumed to be isotropic and constant.

In our case of stationary fields, the Maxwell equations (1) and (2) are decoupled, which means that $\vec{E}$, which causes the current density $\vec{J}_e$, can be expressed by integration of the equation (2):

$$\vec{E} = -\mathrm{grad}\ \phi \qquad (5)$$

where $\phi$ is the electrical scalar potential.

Since the divergence of $\vec{B}$ is zero, the magnetic flux density $\vec{B}$ can be described by a magnetic vector potential $\vec{A}$

$$\vec{B} = \mathrm{curl}\ \vec{A} \qquad (6)$$

Substituting $\vec{H}$ in eq. (1) and using equations (4) and (6), one obtains

$$\mathrm{curl}\ (\nu\ \mathrm{curl}\ \vec{A}) = \vec{J}_e \qquad (7)$$

where $\nu = 1/\mu$ is the magnetic reluctivity.

Introducing vector identities, equation (7) becomes

$$\mathrm{grad}\ \nu \times \mathrm{curl}\ \vec{A} + \nu\ \mathrm{grad}\ \mathrm{div}\ \vec{A} - \nu\Delta\vec{A} = \vec{J}_e \qquad (8)$$

Imposing the condition $\mathrm{div}\ \vec{A} = 0$, we obtain our final differential equation

$$\mathrm{grad}\ \nu \times \mathrm{curl}\ \vec{A} - \nu\Delta\vec{A} = \vec{J}_e \qquad (9)$$

which has to be solved for the magnetic vector potential $\vec{A}$.

The boundary conditions for our problem are restricted to Dirichlet and homogeneous Neumann boundary types.

Using the FEM, the magnetic vector potential $\vec{A}$, the current density $\vec{J}_e$ and the magnetic reluctivity $\nu$ can be expressed by

$$\vec{A} = \sum_{i=1}^{n} N_i\ \vec{A}_i \qquad (10)$$

$$\vec{J}_e = \sum_{i=1}^{n} N_i\ \vec{J}_{ei} \qquad (11)$$

$$\nu = \sum_{i=1}^{n} N_i\ \nu_i \qquad (12)$$

0018-9499/85/1000-3616$01.00© 1985 IEEE

for each finite element.[5] The $N_i$'s are the so-called shape functions[5] which are functions of the local coordinates of a finite element and n is the number of nodes (20 in our case). The $\vec{A}_i$'s are the unknown nodal values of the magnetic vector potential, the $\vec{J}_{ei}$'s and $\nu_i$'s are the known nodal values of the current density and reluctivity, respectively.

Applying Galerkins method and equations (10 to 12) for solving equation (9), we obtain a volume integral over the domain $\Omega$ for each finite element:

$$\int_\Omega N_j \left[ \mathrm{grad}(\sum N_i \nu_i) \times \mathrm{curl}(\sum N_i \vec{A}_i) - \sum N_i \nu_i \Delta (\sum N_i \vec{A}_i) - \sum N_i \vec{J}_{ei} \right] d\Omega = 0 \tag{13}$$

Integrating Equ. (13) by parts and introducing the adequate boundary conditions[3] for the finite elements leads to a set of linear equations which can be written as

$$[k]\{A\} = \{R\} \tag{14}$$

for each finite element. The solving procedure applied in the 3-D FEM software package is the conjugate gradient method preconditioned by an incomplete Cholesky factorization (SICCG)[6].

## Finite element model of the arrangement

The geometry of the dipole is shown in Fig. 3.

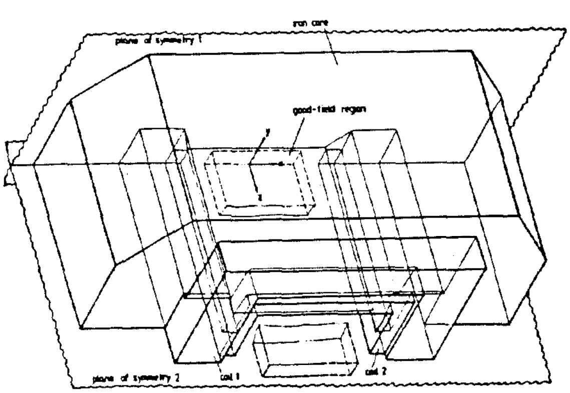


Fig. 3: Model of dipole for numeric field calculations

The final 3-D structure consists of 18 layers with 5184 finite elements. The total number of unknowns (nodal values of components of the magnetic vector potential) is 58500.

## Dipole end fields

The dipole has a magnetic field $\vec{B}$ which varies accross the aperture due to end fields and other perturbations.

In order to respect boundary conditions in the dipole, there is only the vertical component $B_y$ in the median plane x = 0, y = 0. We expand $B_y$ as follows

$$B_y = B_0 \,(1 + b_1 x + b_2 x^2 + \ldots) \tag{15}$$

The odd terms $b_n$ vanish when there is symmetry.

The deviation from uniformity is characterized by

$$\frac{\Delta B_y}{B_0} = \frac{B_y}{B_0} - 1 \tag{16}$$

where $B_0$ is the magnetic field at the centre of the magnet.

For a beam which is passing through a magnet, the relevant quantity is the integrated field through the magnet along the z axis:

$$I_F = \int_{-\infty}^{+\infty} B_y(x,y,z)\, dz \tag{17}$$

The (2n-pole) components of the field are derived from harmonic analysis of the integrated field $I_F$

$$I_F = \int_{-\infty}^{+\infty} B\, dz = \int_{-\infty}^{+\infty} (B_y + iB_x)dz = \sum_{n=0}^{\infty} a_n (x + iy)^n \tag{18}$$

In the median plane $B_x = 0$, therefore

$$I_F = a_0 + a_1 x + a_2 x^2 + a_3 x^3 + \ldots \tag{19}$$

The coefficients $a_0$, $a_1$, $a_2$ ... are called dipole, quadrupole, sextupole ... components.

The variation of $I_F$ is

$$\frac{\Delta I_F}{I_{F0}} = \frac{\int_0^\infty B_y\, dz}{\left( \int_0^\infty B_y\, dz \right)_{\substack{x=0 \\ y=0}}} - 1 \tag{20}$$

For computational convenience, the integrals are taken from the centre of the magnet to infinity.

From the above quantities we define an effective length for the magnet:

$$\ell_{eff} = \frac{1}{B} \int_0^\infty B_y\,(x,\, y,\, z)\, dz \tag{21}$$

and

$$\frac{\Delta \ell_{eff}}{\ell_0} = \frac{\ell_{eff} - \ell_0}{\ell_0} \tag{22}$$

where $\ell_0$ is

$$\ell_0 = \frac{1}{B_0} \int_0^\infty B_y\,(x=0,\ y=0,\ z)\, dz \tag{23}$$

Using equation (19) we have

$$\ell_0 = \frac{a_0}{B_0} \tag{24}$$

The end field contribution begins with $a_1$ (no symmetry) or $a_2$ (with symmetry). The fundamental term $a_0$ is,by definition, included in the effective length.

All variations of these quantities will be considered within the good field region of the dipole, x = ± 186 mm.

## Sextupole term due to end field only

The dipole studied here is a combination of window-frame and H magnet types. The permeability is assumed to be uniform and equal to $\mu_r$ = 531. The current density is constant: coil 1 has $2.469 \times 10^6$ A/m$^2$ and coil 2 has $2.872 \times 10^6$ A/m$^2$.

From Parzen's formula[7], we get

$$b_2 = 7 \times 10^{-3} m^{-2}$$

## Dipole with tilted plate simulating a quadrupole

In this case, there is no symmetry and all terms of equation (15) can be present.

From the results obtained by the model described above, we plot the curve $\Delta B_y/B_0$ versus x (Figure 4).

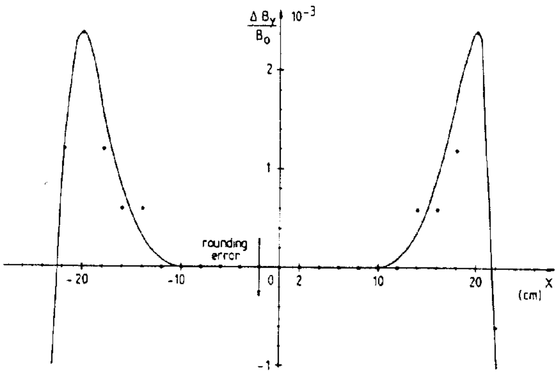


Fig. 4: Magnetic field in the median plane

Within the limited accuracy of this curve (due to limitations from the mesh), the field B in the median plane x=0, y=0, does not depart from $B_0$ up to x = ± 14 cm. The results obtained for the integrated field $I_F$ (Figure 5) are very accurate. The effect of the tilted plate shows up in the slope of the curve.

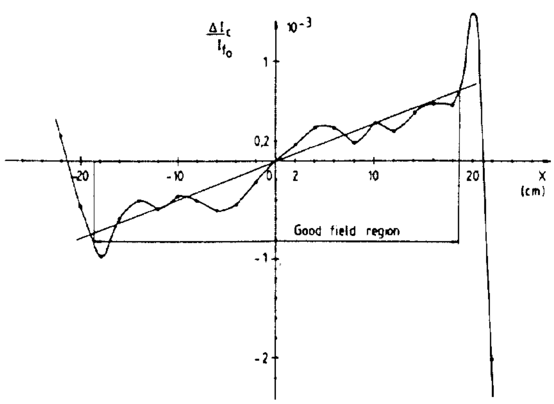


Fig. 5: Integrated field in the median plane

Next, we consider the effective length $\Delta\ell_{eff}/\ell_0$ plotted in Figure 6.

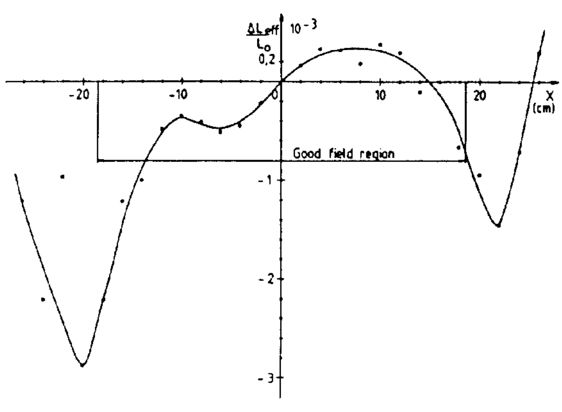


Fig. 6: Effective length in the median plane

Curve fitting for magnetic field, integrated field and effective length give the values summarized in Table 1.

| | Quad. ($m^{-1}$) | Sext. ($m^{-2}$) | Oct. ($m^{-3}$) | Decap. ($m^{-4}$) |
|---|---|---|---|---|
| $\Delta B_y/B_o$ | 0 | 0 | 0 | 1.5 |
| $\Delta\ell_{eff}/\ell_o$ | 9.1 $10^{-3}$ | -0.08 | 2.0 | 58.2 |
| $\Delta I_F/I_{F\,0}$ | 9.1 $10^{-3}$ | -0.09 | 2.0 | 76.4 |

Table 1: Multipole components from the studied configuration

| $\ell_B$ = 0.945 m<br>g = 0.066 m | Units | Theoretical values | At the centre of dipole x = 0 | At the edge of good field region | |
|---|---|---|---|---|---|
| | | | | x = - 18 cm | x = + 18 cm |
| $B_y$ | (T) | 1.600 | 1.637 | 1.639 | 1.639 |
| $\Delta B_y/B_o$ | | | 0 | 1.2 x $10^{-3}$ | 1.2 x $10^{-3}$ |
| $I_F = \int_0^\infty B_y\,dz$ | T.m | 1.56104 | 1.69122 | 1.68958 | 1.69218 |
| $\Delta I_F/IF_o$ | | | 0 | -0.97 x $10^{-3}$ | 0.57 x $10^{-3}$ |
| $\ell_{eff}$ (half dipole) | m | 0.97565 | 1.03312 | 1.03086 | 1.03245 |
| $\Delta\ell_{eff}/\ell_o$ | | | 0 | -2.2 x $10^{-3}$ | -0.65 x $10^{-3}$ |
| $(\ell_{eff} - \ell_B)/g$ | | | | 1.30 | 1.32 |

Table 2 gives a summary of the dipole characteristics pertubed by the vicinity of a tilted plate simulating a quadrupole.

## Conclusion

The results of the computation show errors which are very small and while it is necessary to correct them, this is within the range of correction techniques by shimming used to linearise the field. One obvious improvement might be a full three dimension model of an excited neighbouring magnet.

## Acknowledgements

The authors wish to thank E. Jones for his support and H.H. Umstättter for useful discussions. They also are very grateful to W.M. Rucker and J. Franz at IGTE for helpful collaboration.

## References

[1] ACOL magnets for the design report, L. Rinolfi, PS/AA/AC 16, August 1983.

[2] Design study of an antiproton collector for the antiproton accumulator, edited by E.J.N. Wilson, CERN 83-10, October 1983.

[3] End field of a dipole in presence of a quadrupole arrangement as in the ACOL lattice, L. Rinolfi, H.H. Umstätter (CERN), K. Preis, H. Stögner (IGTE Graz), PS/AA/Note 85-3, January 1985.

[4] Application of higher order finite elements in 3-D magnetic field calculations, H. Stögner, K. Preis, J. Appl. Phys. Vol 53 (1982), p. 8411-8413.

[5] The finite element method, O.C. Zienkiewicz, McGraw-Hill Book Cie, London 1977.

[6] The sifted incomplete Cholesky factorization, T.A. Manteuffel, report No. 9 snd No. 78-8226 Sandia Laboratoris, Albuquerque N.M. (1978).

[7] Magnetic fields for transporting charged beams, G. Parzen, BNL 50536, January 1976.